Journal of Statistical Physics, Vol. 43, Nos. 1/2, 1986

Statistical Properties of the Circle Map

R. V. Jensen[1] and E. R. Jessup[2]

Received July 2, 1985

The circle map provides a generic model for the response of damped, nonlinear oscillators to periodic perturbations. As the parameters are varied this dynamical system exhibits transitions from regular, ordered behavior to chaos. In this paper the regular and irregular behavior of the circle map are examined for a broad range of nonlinearities and frequencies which span not only the regular and transition regimes, which have been studied extensively, but also the strongly nonlinear, chaotic regime. We discuss the bistable behavior (split bifurcations) associated with maps with multiple extrema that gives rise to two disjoint attractors which can be periodic or chaotic and to the low order periodic orbits emerging from chaos via tangent bifurcations. To describe the chaotic behavior we use a statistical description based on a path integral formulation of classical dynamics. This path integral method provides a convenient means of calculating statistical properties of the nonlinear dynamics, such as the invariant measure of the average Lyapunov exponent, which in many cases reduce to analytic expressions or to numerical calculations which can be completed in a fraction of the time required to explicitly iterate the map.

KEY WORDS: Nonlinear dynamics; circle map; period doubling bifurcations; chaos; invariant measures; average Lyapunov exponents; path integrals.

I. INTRODUCTION

Nature exhibits a wide variety of processes with seemingly random behavior. Examples in the biological and physical sciences include such phenomena as population fluctuations among competing species,[1] chemical oscillators, and high Reynold's number fluid flows.[2] Recent attempts to understand and describe these and related dynamical systems have led to the discovery of a special class of deterministic mathematical models. These models, although simple in form, display surprisingly com-

[1] Mason Laboratory, Yale University, New Haven, Connecticut 06520.
[2] Department of Computer Science, Yale University, New Haven, Connecticut 06520.

0022-4715/86/0400-0369$05.00/0

plicated dynamics: as a parameter is varied the observed behavior ranges from orderly and predictable to chaotic. The most extensively studied models are one-dimensional, nonlinear difference equations of the form

$$x_{t+1} = F(x_t, a) \qquad t = 0, 1, 2, 3, \ldots \tag{1}$$

where x_t is the position of the system at some discrete time t, and a provides a measure of nonlinearity.[3] Maps of this type arise as direct models of discrete dynamical systems or as discretizations of differential ones. For strong nonlinearities, i.e., large values of a, these nonlinear maps can exhibit the irregular behavior and the strong dependence on initial conditions characteristic of chaos.[3]

One important example is the circle map

$$x_{t+1} = x_t + a \sin(2\pi x_t) + \Omega \tag{2}$$

which exhibits ordered behavior for small a and undergoes transitions to chaos as a and Ω are varied. This map provides a generic model for the response of nonlinear oscillators to periodic perturbations[4] with applications to problems of cardiac arrhythmia,[5] particle motion in accelerators and magnetic traps,[4] the onset of turbulence in two frequency flows,[6–8] and the dynamics of Josephson junctions and charge density waves in condensed matter physics.[9] The first transition from periodic to chaotic behavior at $a = 1/2\pi$ corresponds to the breakup of Kolmogorof–Arnold–Moser surfaces in higher dimensions[7,8] and has been studied extensively. Little has been written, however, about the behavior of the map for $a > 1/2\pi$. The purpose of this paper is to discuss the regular and irregular behavior of the circle map for $a > 1/2\pi$ and to develop a path integral method for calculating statistical properties of the dynamics in the chaotic regime.

In Section II, we review the behavior of the circle map as a and Ω are varied. (The return map with $\Omega = 0$ is plotted in Fig. 1 for several different values of a.) When $\Omega = 0$, the map undergoes a transition to chaos via a sequence of period-doubling bifurcations accumulating to an aperiodic cycle at $a = a_\infty$.[10] In addition to the usual Feigenbaum bifurcation sequence, this map exhibits the "split bifurcations" characteristic of maps with multiple extrema.[11]

The behavior of Eq. (2) is even richer for $\Omega \neq 0$. (The return map for nonzero Ω corresponds to a vertical translation of Fig. 1 by Ω.) When $a \leqslant 1/2\pi$, the iterates of the map mode-lock to stable periodic attractors. For values of $a > 1/2\pi$, the return map is no longer monotonic and repeated iteration of the map results in stable periodic orbits, chaotic attractors, or a bistable pair of attractors (where one of the two distinct attractors develops depending on initial conditions).[9]

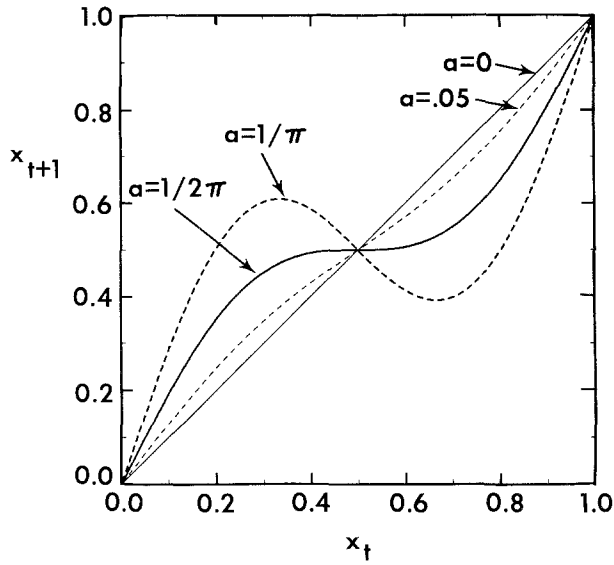

Fig. 1. The return map for Eq. (2) with $\Omega = 0$ is plotted for $a = 0.05$, $1/2\pi$, $1/\pi$. The return map for $\Omega \neq 0$ corresponds to vertical translation by Ω.

For most values of $a > a_\infty$, when $\Omega = 0$, and for $a > 1/2\pi$, when $\Omega \neq 0$, the map exhibits the extreme sensitivity to initial conditions characteristic of chaotic behavior. Within this chaotic regime, however, the bifurcation diagram for the circle map also includes numerous periodic windows. For example, we note that when $\Omega = 0$ a single period-2 cycle appears near half-integer values of a, while one of two stable fixed points emerges depending on the initial condition for integer values. In both cases, a sequence of period-doubling bifurcations and return to chaos are observed on all periodic attractors as a is increased. The bistable behavior also persists in the chaotic regime where competition occurs not only between two periodic orbits or two chaotic attractors but also between periodic and chaotic attractors when $\Omega \neq 0$.

When the motion is chaotic, the complexity of the dynamics suggests that a statistical description is appropriate. In Section III, we exploit a path-integral formalism to calculate important statistical quantities such as the long-time probability distribution and the average Lyapunov exponent which characterizes the stochastic instability.

The path integral method for classical dynamics was first applied in renormalized perturbation theories to calculate the statistical correlation and response functions describing fluid and plasma turbulence.[12–15] The most notable success, however, has been in the explicit calculation of

statistical properties of dynamical systems modeled by nonlinear difference equations.[16–24] In particular, the path integral method can be used to accurately determine the asymptotic probability distribution for the circle map. Periodic orbits are represented by prominent and correctly positioned extrema in the plots of probability distribution versus x while the invariant measures for chaotic orbits are smooth distributions with peaks located at the images of the critical points of the map.[25] In the event of two possible attractors, the analytic result includes both, corresponding to the probability measure left invariant by the dynamics without regard to the specific initial conditions. Finally, the probability distribution is used to evaluate the average Lyapunov exponent.[26] Analytically and numerically determined values for the invariant measure and the average Lyapunov exponent are in excellent agreement.

II. REGULAR AND CHAOTIC BEHAVIOR

A. Weak Nonlinearity

When $\Omega = 0$, the circle map undergoes a transition from stable periodic attractors to chaotic attractors as a is increased. This transition takes the form of a sequence of period doubling and "split" bifurcations. Figures 2a and 2b show bifurcation diagrams for $\Omega = 0$ and $0 \leqslant a \leqslant 1.51$ for two different initial conditions lying in different basins of attraction. For small a, the successive iterates of the map are attracted to a stable fixed point at $x = 0.5$ that bifurcates into a period-2 cycle at $a = 1/\pi$. When a is increased beyond 0.5, four stable period-2 points appear, and the long-time dynamics lie on one of two distinct period-2 cycles depending on the initial condition x_0. This bistable behavior is registered on the bifurcation diagram as a split bifurcation. Similar split bifurcations have also been observed for the cubic map.[11] In general, maps with n extrema can have up to n different attractors with disjoint basins of attraction.[11]

The subsequent period-doubling bifurcations on each branch of the split bifurcation can be described using the standard techniques developed by Feigenbaum and others for one-dimensional difference equations with a single, locally quadratic extremum.[3,10] Each branch undergoes a sequence of period-doubling bifurcations beginning with a pitchfork bifurcation to a stable 4-cycle at $a_4 = (0.25 + 1/2\pi^2)^{1/2} \approx 0.5483$,[5] followed by a bifurcation to a stable 8-cycle at $a_8 \approx 0.5590$, and leading to an eventual aperiodic cycle at the accumulation point a_∞. Using the Feigenbaum number, $\delta \approx 4.669$, and the difference $a_8 - a_4 = 0.0107$, a_∞ can be estimated by

$$a_\infty \approx 0.5483 + 0.0107 \sum_{n=0}^{\infty} \left(\frac{1}{4.669}\right)^n = 0.562 \tag{3}$$

When $\Omega = 0$, the a values at the accumulation point as well as at all preceding bifurcations are the same on both branches of the split bifurcation.

The addition of a nonzero Ω results in a significant change in the prechaotic scenario for the circle map. When $a = 0$, the time evolution is quasi-periodic for almost every Ω; the map exhibits periodic behavior only

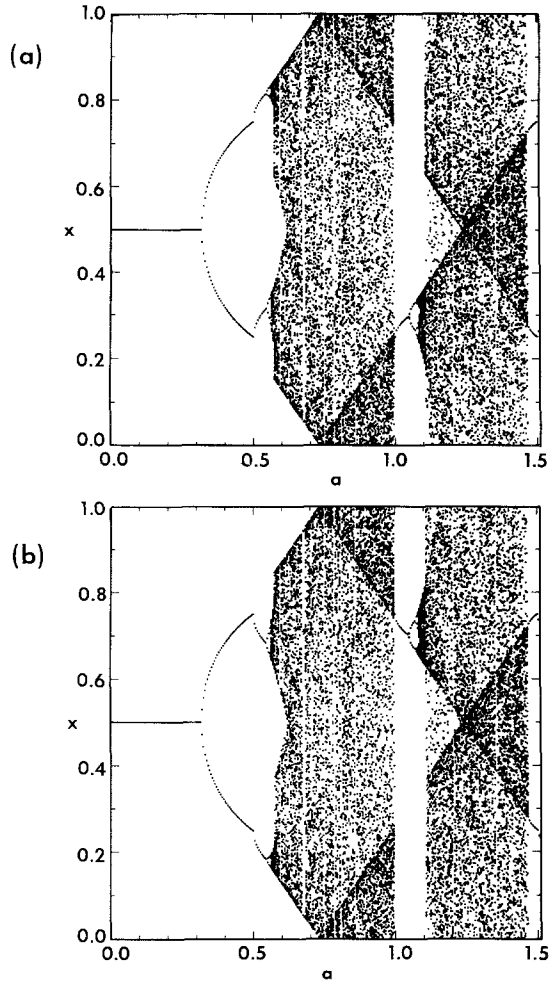

Fig. 2. The long time iterates of the circle map are plotted for $\Omega = 0$ and for values of a between 0.0 and 1.51 to generate the bifurcation diagrams for two different initial conditions, (a) $x_0 = 0.25$ and (b) $x_0 = 0.75$, showing the bistable behavior associated with the multiple extrema of the circle map. The map was evaluated modulo one to extend the bifurcation diagram beyond $a = a_d \simeq 0.7326$.

for rational values of Ω. For nonzero a, however, "mode-locking" to stable periodic attractors occurs for bands of Ω which increase in size with increasing a. These mode-locking bands are called Arnold "tongues" and cover roughly triangular regions in a plot of a versus Ω. (See Fig. 2 of Ref. 5). Between the Arnold tongues the motion is quasi-periodic. When $a = 1/2\pi$, the successive iterates converge to a periodic cycle for almost every Ω, and the Arnold tongues consume the entire range of Ω. Furthermore, because every rational period occurs for some value of Ω, a graph of the winding number

$$W = \lim_{N \to \infty} \frac{x_N - x_0}{N} \tag{4}$$

plotted as a function of Ω forms a complete "devil's staircase."[9]

For $a > 1/2\pi$, the dynamics become quite complicated. Period-doubling bifurcations, bistability, and chaos have been observed numerically as well as experimentally in situations modeled by the circle map.[9] The transition from regular to irregular behavior at $a = 1/2\pi$ corresponds to the point at which the return map, Eq. 2, ceases to be a monotonic function of x_t. When $a \leqslant 1/2\pi$, the circle map can always be transformed to a regular rotation, but when $a \geqslant 1/2\pi$, the coordinate transformation breaks down. This failure corresponds to the breakup of Kolmogorof–Arnold–Moser surfaces in two-dimensional maps and has been shown, through a renormalization group analysis, to display universal properties.[7,8]

B. Strong Nonlinearity

Some of the effects of large nonlinearity are revealed in an examination of the circle map for $\Omega = 0$. For most values of $a > a_\infty$, the dynamics exhibit the extreme sensitivity to initial conditions characteristic of chaotic dynamical systems. Neighboring trajectories no longer converge to periodic cycles but split apart at an exponential rate. For one-dimensional difference equations like Eq. (1), the average Lyapunov exponent, defined as

$$\lambda = \lim_{N \to \infty} \frac{1}{N} \sum_{t=0}^{N} \ln \left[\left| \frac{dF}{dx}(x_t) \right| \right] \tag{5}$$

provides a measure of the local instability.[27] As can be seen in Fig. 3, λ first becomes positive for $a > a_\infty$. The negative spikes correspond to the reemergence of periodic attractors. Pesin has proven that positive Lyapunov exponent is equivalent to positive Kolmogorof entropy.[28] Thus, chaotic dynamical systems with $\lambda > 0$ are by definition "mixing" systems or, more precisely, K systems.[29]

For $a < a_d = 0.7326...$, the successive iterates of the circle map are confined to a subset of the unit interval. The motion first spans the entire interval $[0, 1]$ at $a = a_d$. For values of a between a_∞ and a_d, the dynamics of the circle map are similar to that of the celebrated logistic map.[10] The chaotic regime is filled with small intervals of a where the motion converges to periodic cycles. The larger of these intervals can be clearly seen as gaps in the bifurcation diagrams, Fig. 2a and 2b, and as negative spikes in the graph of the average Lyapunov exponent as a function of a, Fig. 3. These periodic cycles emerge as tangent bifurcations and dissolve into chaos through a sequence of period-doubling bifurcations. Because of the two extrema, the order of appearance of the cycles of different periods is not the same as for the logistic map,[11] and the subsequent period doubling of the circle map includes split bifurcations and the associated bistability.[11]

Although the intervals of regular behavior appear to densely cover the entire range of a, Jakobson has proven for the logistic map that the values of a giving rise to chaotic behavior form a set of nonzero measure.[3,30] A similar conclusion may be expected for the circle map. Consequently, when the motion appears to be chaotic it is possible (perhaps likely) that it is actually chaotic and not just a periodic cycle with an extremely long period. Once again, the main difference between the chaotic behavior of the

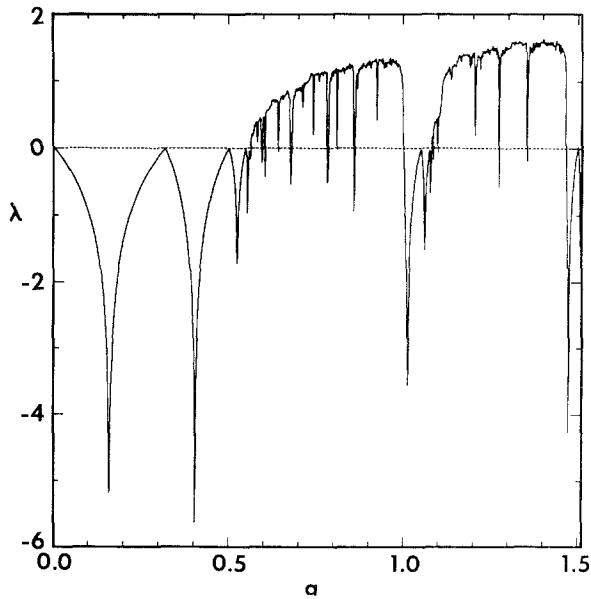

Fig. 3. The average Lyapunov exponent for the circle map, computed from Eq. (5), is plotted as a function of a between 0.0 and 1.51.

circle map and unimodal maps is the persistence of bistability. At many values of a following the appearance of a periodic orbit, the map exhibits pairs of chaotic attractors as well as pairs of periodic orbits with disjoint basins of attraction. (See, for example, Figs. 2a and 2b.) These basins coalesce, however, at the crisis points[31] where the chaotic bands of the two attractors intersect at an unstable periodic orbit.[11]

When $a > a_d$, the dynamics of the circle map become unbounded. The chaotic orbits exhibit a diffusive behavior characterized statistically by a mean square displacement $\langle (x_t - x_0)^2 \rangle$ which grows steadily with time.[32] However, since we are mostly concerned with equilibrium statistical properties of the circle map, it is convenient to take advantage of the natural periodicity of the map and treat x_t as an angle variable restricted to the interval [0, 1]. This is easily accomplished by defining the circle map, Eq. (2), modulo 1. With this definition, orbits that would escape from the unit interval are folded back in as seen in Figs. 2a and 2b for $a > a_d$.

When a is greater than or equal to 1.0, periodic attractors emerge from chaos at integer and half-integer values of a. When a is an integer, the circle map (defined modulo 1 with $\Omega = 0$) exhibits a tangent bifurcation to a pair of period-1 fixed points at $x = 0.25$ and $x = 0.75$. Only one of these attractors appears for any single initial condition (see Figs. 2a and 2b), and both undergo simultaneous sequences of pitchfork bifurcations to chaos. The long-time orbits for values of a near 1 are shown in Fig. 4.

The emergence of order from chaos near half-integer values of the nonlinear parameter differs in structure from the former case. A single stable 2-cycle emerges through a tangent bifurcation when a is slightly less than a half-integer. At the half-integer value of a, a split bifurcation occurs, resulting in a pair of new and independent period-2 cycles. Then, as observed for a larger than 0.5, a sequence of period doubling bifurcations leads to chaos on each of the separate attractors. The bifurcation diagram for values of a near 1.5 is displayed in Fig. 5.

We note that periodic orbits are not the only regular structures visible in the bifurcation diagrams within the chaotic regime. Dark streaks corresponding to regions of high probability also appear (see Figs. 2a and 2b). The locations of these smooth structures are determined by the images of the extrema of the map.[25] Because the invariant measure, $P_I(x)$, associated with the chaotic dynamics is formally determined by the relation[26]

$$P_I(x) = \sum_i \frac{P_I(x_i)}{|(dF/dx_i)(x_i)|} \tag{6}$$

where the x_i denote the pre-images of the point x, the probability distribution diverges at the images of the extremal points of the map. If the

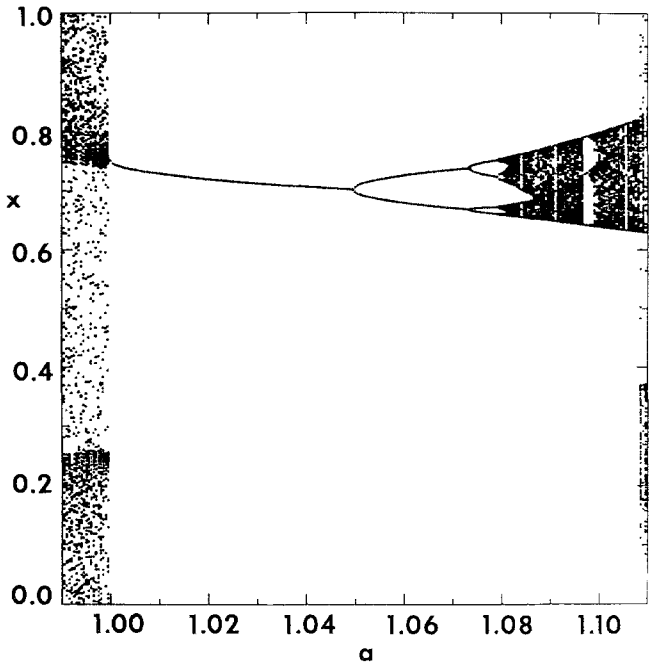

Fig. 4. The bifurcation diagram for $\Omega = 0$ and $x_0 = 0.75$ is magnified for values of a near 1. A period-1 attractor emerges at $a = 1.0$ and undergoes its first period-doubling bifurcation at $a = 1.05$. It becomes an aperiodic attractor at the accumulation point at $a_\infty \approx 1.08$. The other period-1 fixed point appears at $a = 1.0$ for values of x_0 in its basin of attraction, such as $x_0 = 0.25$, and bifurcates to chaos in an identical fashion.

invariant measure is nonzero at these critical points, the distribution exhibits an integrable singularity of the form $1/|x - F^n(x^*)|^{1/2}$ at each of the n images of the critical points x^*. In Section III, we present a path-integral method which provides an alternate method for explicitly calculating the full invariant measure.

Finally, although the large a behavior of the circle map for nonzero Ω is qualitatively similar, the ordering of periodic cycles and chaotic attractors for large a varies with Ω. For example, when a is large, split bifurcations can give rise to a pair of disjoint attractors with different periods, and competition can occur between a periodic cycle and a chaotic one. Examples of split bifurcations leading to regular or chaotic attractors depending on the initial condition are illustrated in Figs. 6a and 6b.

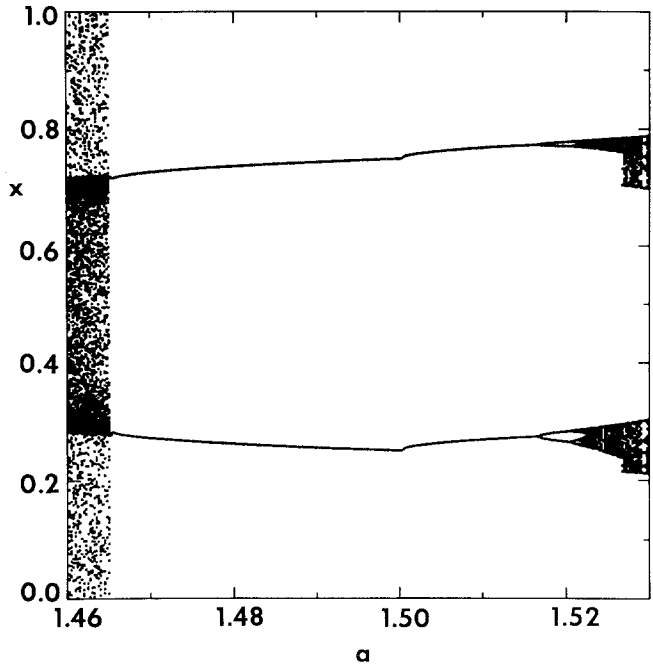

Fig. 5. The bifurcation diagram for $\Omega = 0$ and is magnified for values of a near 1.5. When $a \simeq 1.465$, a single period-2 cycle appears. At $a = 1.5$, a split bifurcation takes place and gives rise to a pair of degenerate period two cycles that alternate between $x = 0.25$ and $x = 0.75$. Then both pairs of attractors cascade back to chaos via simultaneous sequences of period doubling bifurcations.

III. CALCULATION OF STATISTICAL PROPERTIES OF THE CIRCLE MAP

In general, the long-time behavior of nonlinear dynamical systems, like that of the circle map, cannot be determined analytically. The equations of motion are nonintegrable, and the conventional analytic methods based on perturbation theories fail for large nonlinearities. Fortunately, analytic means can often be devised to account for observations of such regular behavior as periodic cycles or prominent peaks in the invariant measure. Several successful analyses of the regular behavior of the circle map were discussed in the previous section.[5–9,25] However, when the motion is chaotic a description in terms of the individual orbits is not only analytically intractable but also unserviceable due to the extreme sensitivity of the dynamics to the initial conditions. In this case, a statistical description in terms of an ensemble of initial conditions is more appropriate and

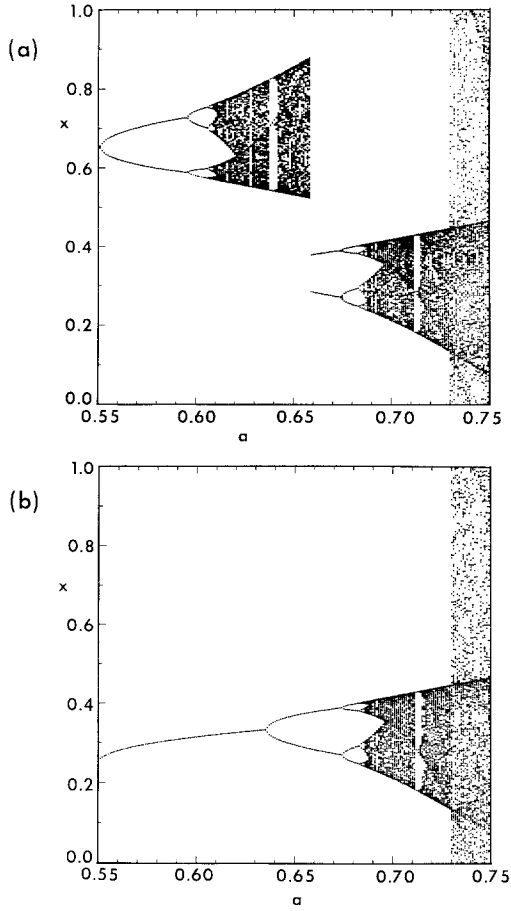

Fig. 6. The bifurcation diagrams displaying the competing attractors are shown for $\Omega = 0.45$ and values of a between 0.55 and 0.75. The long-time, regular, and chaotic behavior for $x_0 = 0.75$ is shown in (a), while the bifurcation diagram for $x_0 = 0.25$ is shown in (b). This figure shows that for $\Omega \neq 0$ the bistable behavior can occur between two periodic attractors, two chaotic attractors, or one periodic and one chaotic attractor. Near $a = 0.65$ a "crisis" occurs and the two attractors coalesce into one.

may admit an analytic treatment of the chaotic dynamics if the appropriate probability distributions can be determined.

To this end, a path integral method[16-24] has been developed to provide an efficient, semianalytic means of calculating observable statistical properties of chaotic systems. Using the path integral representation of classical dynamical systems,[15] functionals of the dynamics, such as correlation functions and conditional probability distributions, are determined by the evaluation of integrals rather than the solution of differential

or difference equations. These path integrals provide a useful description of systems exhibiting chaotic behavior due to external noise or intrinsic stochasticity. Moreover, the functional integrals arising in statistical dynamics are very similar to those in quantum theory and statistical mechanics. Consequently, analytic techniques developed in the latter areas can be extended to problems in chaotic dynamics.

One immediate application of the path integral method is to the calculation of the stationary probability distribution for chaotic dynamical systems.[22–24] This distribution $P_I(x)$ is defined as the measure left invariant by the dynamics. For discrete dynamical systems, the semigroup property of the conditional probability leads to an integral representation for the invariant measure

$$P_I(x_{t+1}) = \int dx_t \, P(x_{t+1} | x_t) \, P_I(x_t) \tag{7}$$

where $P(x_{t+1} | x_t)$ is the conditional probability for a transition from x_t to x_{t+1}. For the deterministic process defined by Eq. 1, $P(x_{t+1} | x_t)$ is given simple by a Dirac delta function $\delta(x_{t+1} - F(x_t))$.

If the dynamics are chaotic, then Eq. 7 determines a smooth probability measure which is absolutely continuous with respect to Lebesgue measure. However, if the long-time dynamics lie on a stable periodic orbit, then the solution of Eq. (7) will consist of a sequence of Dirac δ functions centered on the elements of the periodic cycle, and approximate solutions of Eq. 7 will give approximate representations of these δ functions. Moreover, if there are several invariant measures corresponding to different attractors, as is often the case for the circle map, then the solution for P_I will be a linear superposition of all of these measures.

When x_t is bounded on a finite interval, as for the circle map, the delta function can be expanded as a Fourier series, thereby transforming Eq. (7) into a form reminiscent of the path integrals appearing in quantum theories,

$$P_I(x_{t+1}) = \sum_{m=-\infty}^{\infty} \int_0^1 dx_t \, P_I(x_t) \, e^{i2\pi m(x_{t+1} - F(x_t))} \tag{8}$$

Replacing P_I on both sides of Eq. (8) by its Fourier transform

$$A(n) = \int_0^1 dx \, e^{-i2\pi xn} P_I(x) \tag{9}$$

we get in a relation for the Fourier components of the stationary probability distribution

$$A(n) = \sum_{m=-\infty}^{\infty} M(n, m) \, A(m) \tag{10}$$

where

$$M(n, m) = \int_0^1 dx\, e^{i2\pi(mx - nF(x))} \tag{11}$$

Equation (10) is an infinite-dimensional matrix equation

$$A = MA \tag{12}$$

where $A_n = A(n)$ is the eigenvector with unit eigenvalue[23] of the matrix $M_{nm} = M(n, m)$. If the matrix elements decay rapidly enough for large mode numbers, as is often the case for chaotic dynamical systems, the matrix system may be truncated and solved analytically or numerically for the values of the Fourier coefficients. The invariant probability distribution can then be constructed by inverting the Fourier transform

$$P_I(x) = \sum_{n=-\infty}^{\infty} e^{i2\pi nx} A(n) \tag{13}$$

As an illustration, consider the tent map

$$x_{t+1} = \begin{cases} 2x_t & \text{if } 0 \leqslant x_t \leqslant 0.5 \\ 2(1 - x_t) & \text{if } 0.5 \leqslant x_t \leqslant 1.0 \end{cases} \tag{14}$$

which was first proven to have a uniform stationary distribution on the interval [0, 1] by Kac.[33] For this example, Eq. (11) gives

$$M(n, m) = \int_0^{0.5} dx\, e^{i2\pi x(m-2n)} + \int_{0.5}^1 dx\, e^{i2\pi x(m+2n)} \tag{15}$$

Then using Eq. (10) and the condition $A^*(n) = A(-n)$, which guarantees a real value of $P_I(x)$, we get

$$\operatorname{Re} A(n) = \sum_{m=-\infty}^{\infty} [\delta_k(m-2n) + \delta_k(m+2n)]\, A(m) \tag{16}$$

Since the Kronecker δ_k functions are real, all terms $A(n)$ must also be real. Therefore, Eq. (16) requires that

$$2A(n) = A(2n) + A(-2n) = 2A(2n) \tag{17}$$

This relation is satisfied by $A(0) = \int_0^1 P_I(x)\, dx \equiv 1$; and for all $n \neq 0$, Eq. (17) dictates that $A(n) = c$, where c is an undetermined constant. Then from Eq. (13) we find

$$\begin{aligned} P_I(x) &= \sum_{n=-\infty}^{\infty} A(n)\, e^{i2\pi nx} = (1-c) + c \sum_{n=-\infty}^{\infty} e^{i2\pi nx} \\ &= (1-c) + c \sum_{n=-\infty}^{\infty} \delta(x-n) \end{aligned} \tag{18}$$

Consequently, the only nonsingular probability distribution is the uniform distribution $P(x)=1$ corresponding to $c=0$.

The invariant distribution of the circle map, Eq. (2), can be calculated in a similar manner. In this case

$$M(n, m)=\int_0^1 dx\, e^{i2\pi[x(m-n)-n(a\sin 2\pi x+\Omega)]}=e^{-i2\pi n\Omega}J_{m-n}(2\pi na) \quad (19)$$

where $J_n(z)$ is the ordinary Bessel function of the first kind of order n. The Fourier coefficients of the invariant measure are then determined by Eq. (10)

$$\begin{aligned} A(n)&=\sum_m e^{-i2\pi n\Omega}J_{m-n}(2\pi na)\,A(m)\\ &=e^{-i2\pi n\Omega}J_{-n}(2\pi na)\,A(0)+\sum_{m\neq 0} e^{-i2\pi n\Omega}J_{m-n}(2\pi na)\,A(m) \end{aligned} \quad (20)$$

As above, $A(0)\equiv 1$, and a series representation of each coefficient can be obtained by iterating the sum in the second term.[22] For example, when $\Omega=0$

$$\begin{aligned} A(n)&=J_{-n}(2\pi na)+\sum_{m\neq 0} J_{m-n}(2\pi na)\,J_{-m}(2\pi ma)\\ &\quad+\sum_{m\neq 0}\sum_{q\neq 0} J_{m-n}(2\pi na)\,J_{q-m}(2\pi ma)\,J_{-q}(2\pi qa)+\cdots \end{aligned} \quad (21)$$

For $a\gg 1$, the Bessel functions may be replaced by their asymptotic forms.[34]

$$J_{m-n}(2\pi na)\approx\frac{1}{\pi\sqrt{na}}\cos\left(2\pi na-\frac{(m-n)\pi}{2}-\frac{\pi}{4}\right) \quad (22)$$

Then, to leading order in $1/\sqrt{a}$

$$A(n)\approx J_{-n}(2\pi na)\,e^{-i2\pi n\Omega} \quad (23)$$

and the invariant distribution reduces to

$$P_I(x)=1+2\sum_{n>0}\cos[2\pi n(x-\Omega)]\,J_{-n}(2\pi na) \quad (24)$$

A plot of $P_I(x)$ over the interval $[0, 1]$ is shown by the dashed curve in Fig. 7 for $a=10.6$. While gross structure is revealed with fewer than 10 terms, the infinite sum has been truncated to 50 terms, the minimum number required to produce most discernable structure. A smaller number of

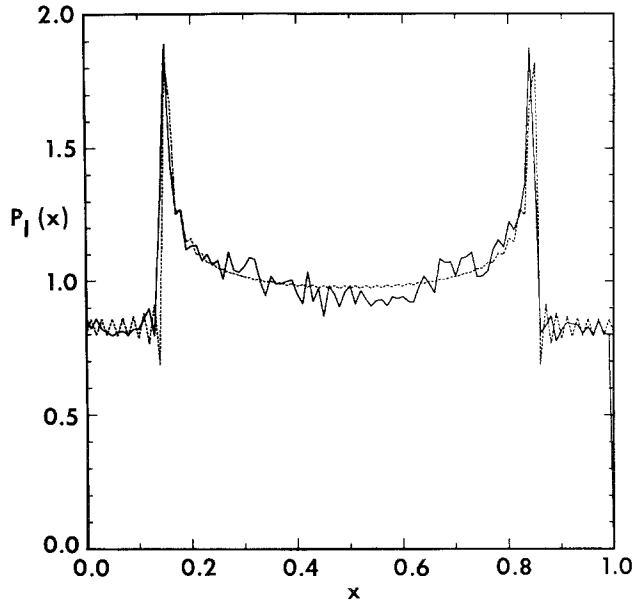

Fig. 7. The invariant probability distribution is shown for the circle map for $\Omega = 0$ and a large nonlinearity, $a = 10.6$. The solid curve was determined by iterating the map 100,000 times and constructing a histogram by dividing the unit interval into 100 bins. The analytic approximation based on Eq. (24) with 50 terms is superimposed as a dotted line.

terms is required for larger values of a. In the same figure, the validity of the approximation is confirmed through comparison with the numerically determined probability distribution (solid curve) which was computed by iterating the map 100,000 times and constructing a histogram of the number of occurrences of different values of x.

For small values of a, Eq. (24) no longer provides a good approximation to the invariant measure; and the coefficients $A(n)$ must be obtained directly from a truncated form of Eq. (12) where the Bessel functions are evaluated exactly. For most values of a studied, a 101×101 matrix system is sufficient to reproduce the structure of the calculated invariant distribution. (In actual calculations the size of the system can be further reduced using the symmetries of the Fourier coefficients and the fact that $A(0) = 1$.)

Good correspondence between numerical and analytical results is obtained through a range of small a values. For example, Fig. 8 shows a comparison of the histogram with the invariant measure determined from the solution of Eq. (12) for $a = 0.91$. Despite its complexity, the structure of the histogram plot is closely reproduced by the calculated $P_I(x)$.

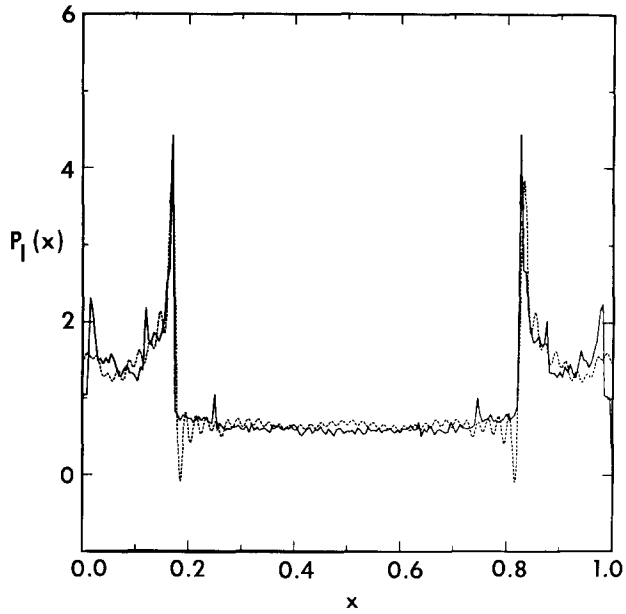

Fig. 8. The invariant probability distribution is shown for the circle map for $\Omega = 0$ and a small nonlinearity, $a = 0.91$. The solid curve corresponds to a histogram constructed by iterating the map 100,000 times. The path integral result using Eq. (12) truncated to 101 terms is superimposed as a dotted line.

The solution of the matrix equation can also be used to calculate the properties of the long-time behavior of the map before as well as after the onset of chaos. In Fig. 9, for example, the analytically determined distribution for $a = 0.45$ and $\Omega = 0$ is superimposed upon the numerical result for the same parameters. The sharp peaks of both distributions correspond to the regular period-2 cycle. In addition, Fig. 10 shows the invariant measure for $a = 0.505$. For this value of a the bifurcation diagrams, Figs. 2a and 2b, show two distinct 2-cycles and the histogram, shown by the solid curve in Fig. 10, exhibits the two prominent extrema for one of the period-2 attractors corresponding to $x_0 = 0.75$. Displaying the second attractor requires use of a starting value within its basin of attraction. However, the path integral result, indicated by the dashed curve, depends only on the unique solution of Eq. (12) and includes the peaks of both possible attractors.

The path integral method is equally effective for the calculation of the invariant measure for the circle map with nonzero Ω. For example Fig. 11 shows the approximate invariant measure corresponding to the appearance of a disjoint pair of periodic and chaotic attractors for the values of a and

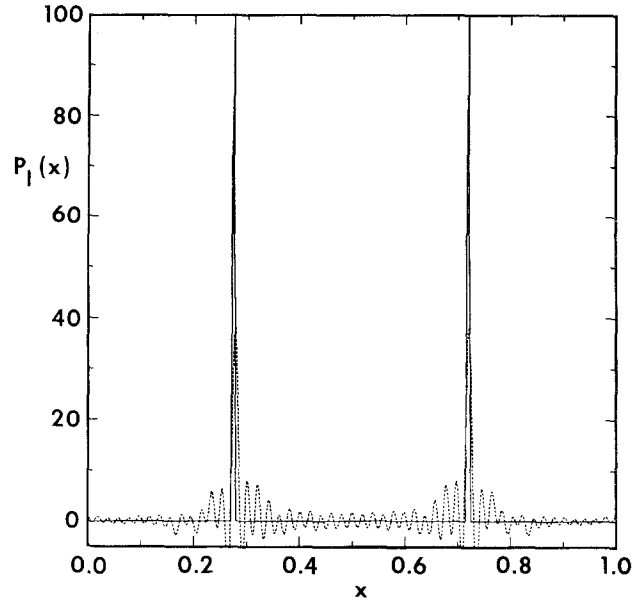

Fig. 9. The invariant probability distribution for a period-2 orbit is shown for $\Omega = 0$ and $a = 0.45$. The solid curve corresponds to a histogram constructed by iterating the map 100,000 times. The path integral result using Eq. (12) truncated to 101 terms is superimposed as a dotted line.

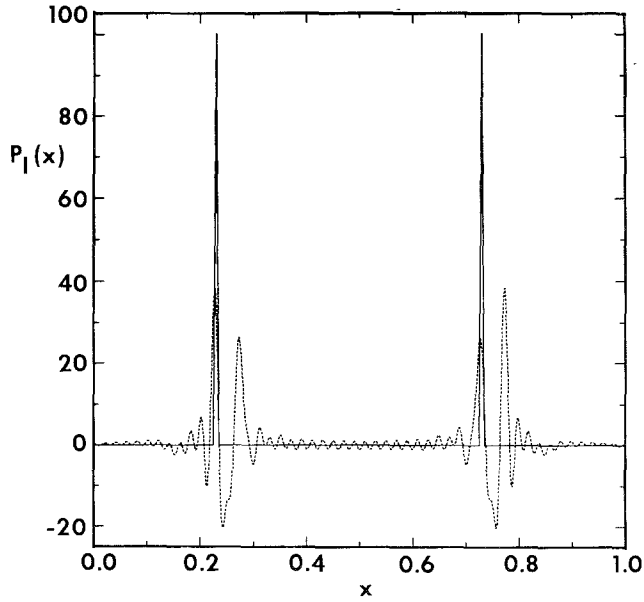

Fig. 10. The invariant probability distribution is shown for the circle map for $\Omega = 0$ and $a = 0.505$. The solid curve corresponding to the histogram, constructed by iterating the map 100,000 times from a single initial condition, shows only one branch of the two bistable, period-2 attractors while the path integral result using Eq. (12) truncated to, indicated by the dotted curve, captures both periodic attractors.

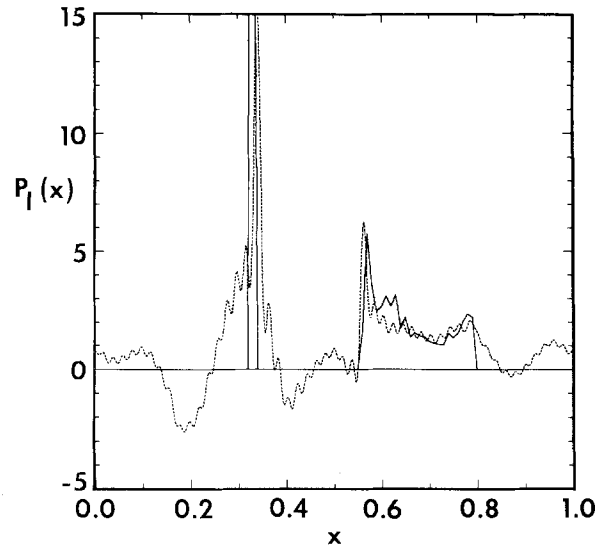

Fig. 11. The invariant probability distribution is shown for the circle map for $\Omega = 0.45$ and $a = 0.62$. The solid line shows the histograms for the two disjoint attractors, one periodic on the left and one chaotic on the right, constructed by iterating the map 100,000 times for two different initial conditions. The path integral result using Eq. (12) truncated with 101 terms, which is indicated by the dotted line, provides a representation of both attractors.

Ω used in Figs. 6a and 6b. As before, the truncated solution of Eq. (12) captures both attractors, whereas, the iteration of the map provides a histogram of one or the other depending on the initial condition.

Finally, this method is also useful for calculating statistical properties other than the probability distribution. For example, in a chaotic system, an infinitesimal error in the initial position of a trajectory leads to great uncertainty in the position at any later time. Neighboring orbits split apart at an exponential rate. The average Lyapunov exponent λ provides a measure of this divergence.[27] The average Lyapunov exponent is easily determined using the calculated probability distribution. For the circle map with $\Omega = 0$ and $a \gg 1$

$$\begin{aligned}\lambda &= \int_0^1 dx\, P(x) \ln \left| \frac{dF}{dx} \right| \\ &= \int_0^1 dx \left[1 + 2 \sum_n \cos(2\pi n x)\, J_n(2\pi n a) \right] \ln \left| \frac{dF}{dx} \right| \\ &\approx \ln(\pi a) + O(\ln a/\sqrt{a}) \end{aligned} \tag{25}$$

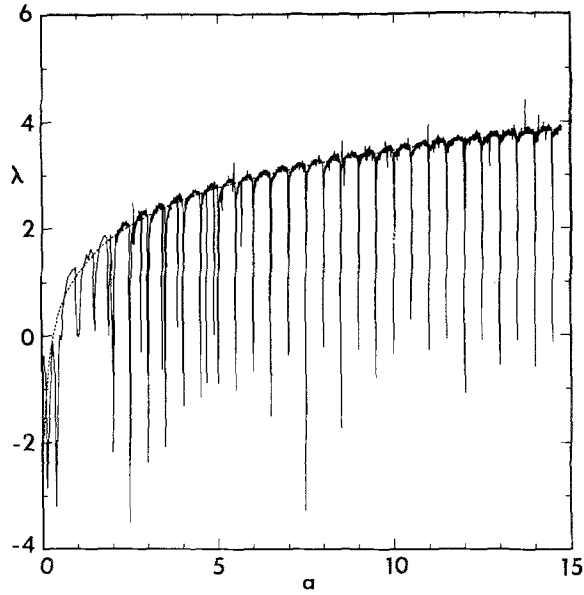

Fig. 12. A comparison of the theoretical estimate for the average Lyapunov exponent, Eq. (25), with the numerically calculated values over a broad range of nonlinearities. The theoretical estimate is shown by the dotted curve while the numerical result is given by the solid curve. Except for the periodic orbits at $a < 1$ and at integer and half-integer values of a, which are indicated by the negative spikes in the solid curve, the agreement is excellent.

This approximate result is identical to that obtained by Chirikov for the two-dimensional extension of the circle map known as the standard map.[35] Although the leading term in this expansion is equivalent to a random phase average, the path integral result also provides a systematic expansion of the corrections to the random phase approximation.

As shown in Fig. 12, Eq. (25) gives a close representation of the numerically determined Lyapunov exponent plotted against the parameter a for a wide range of a values. Large deviations occur only near the known positions of fixed points of the map. The virtue of this result is that the Lyapunov exponent can be estimated without the use of a computer. Similar analytic formulas can also be derived for other statistical quantities dependent on the probability distribution or its Fourier coefficients.

IV. CONCLUSION

Although the circle map has received a tremendous amount of attention in a wide variety of applications, very little has been written about the

behavior of the map in the strongly nonlinear regime, $a > 1/2\pi$, which exhibits a complicated mixture of periodic orbits, chaos, and bistability. In an attempt to mitigate this deficiency, we have provided a discussion of some of the possible behaviors of the strongly nonlinear circle map including split bifurcations, the emergence of periodic orbits at integer and half-integer values of a, and the possibility of two disjoint attractors which can be either regular or chaotic. In addition, we have applied a path integral method to calculate various statistical properties of the dynamics of the circle map in this regime.

The path integral method is particularly useful for calculating the invariant probability distribution which describes the long-time behavior of the map. For large values of a the invariant measure is determined by a series expansion in terms of ordinary Bessel functions. For smaller values of $a \leqslant 1$ the series expansion converged too slowly, and it was necessary to solve a truncated system of linear equations for the Fourier coefficients of the invariant measure. In both cases the results showed good agreement with the histograms constructed by iterating the map for 10^5 time steps and could be evaluated in a fraction of the computer time required for the explicit simulation. Moreover, once the invariant measure is known, then other long-time statistical quantities are easily evaluated. These include the average Lyapunov exponent, which was found to be in excellent agreement with the numerical results.

The success of the path-integral method for the description of the chaotic dynamics can be attributed to the fact that properties of strongly nonlinear systems are calculated by performing a steepest descent integral where the strength of the nonlinearity plays the role of the asymptotic parameter. Moreover, the representation of the probability distribution in terms of its Fourier components simplifies calculations for chaotic systems since the chaotic invariant measure tends to be relatively smooth in real space, thereby requiring fewer Fourier components for its accurate representation. The probability distribution for periodic orbits, on the other hand, is highly localized to a sequence of Dirac δ functions which are not well represented by a finite number of Fourier components. Nevertheless, the probability distributions calculated with 101 Fourier components were found to provide an excellent approximation to the singular invariant measures associated with periodic orbits such as the period-2 cycle at $a = 0.45$.

Finally, we emphasize that the path integral method described here can be used to calculate the invariant measures for many different maps in one or more dimensions as long as the dynamics are restricted to a bounded region of phase space. Moreover, a more general form of the path integral method can also be used to calculate conditional and time-depen-

dent probability distributions which determine the time evolution of observable, statistical properties of the nonlinear dynamical systems such as correlation functions and diffusion coefficients.[16–19]

ACKNOWLEDGMENTS

This work was supported in part by the National Science Foundation under Grant Number PHY830-8280 and the Office of Naval Research under Grant Number N00014-83-K-0610.

REFERENCES

1. R. M. May, *Nature* **261**:459 (1976).
2. See papers in *Physica* **7D**:1–362 (1983).
3. P. Collet and J.-P. Eckmann, *Iterated Maps on the Interval as Dynamical Systems* (Birkhauser, Boston, 1980).
4. G. M. Zaslavskii and Kh.-R. Ya. Rachko, *JETP* **49**:1039 (1979).
5. L. Glass and R. Perez, *Phys. Rev. Lett.* **48**:1772 (1982).
6. P. Coullet, C. Tresser, and A. Arneodo, *Phys. Lett.* **77A**:327 (1980).
7. D. Rand, S. Ostlund, J. Sethna, and E. D. Siggia, *Phys. Rev. Lett.* **49**:132 (1982).
8. S. J. Shenker, *Physica* **5D**:405 (1982).
9. M. H. Jensen, P. Bak, and T. Bohr, *Phys. Rev.* **30**:1960 (1984).
10. P. Cvitanovic, *Universality in Chaos* (Adam Hilger, Bristol, Great Britain, 1984).
11. J. Testa and G. A. Held, *Phys. Rev.* **A28**:3085 (1983).
12. C. DeDominicis, *J. Phys. (Paris)* **C1**:247 (1976).
13. H. K. Janssen, *Z. Phys.* **B23**:377 (1976).
14. R. Jouvet and R. Phythian, *Phys. Rev.* **A19**:1350 (1979).
15. R. V. Jensen, *J. Stat. Phys.* **25**:183 (1981).
16. R. V. Jensen and C. R. Oberman, *Phys. Rev. Lett.* **46**:1547 (1981).
17. R. V. Jensen and C. R. Oberman, *Physica* **4D**:183 (1982).
18. A. B. Rechester, R. B. White, and M. Rosenbluth, *Phys. Rev.* **23A**:2664 (1981).
19. H. D. J. Abarbanel and J. D. Crawford, *Physica* **5D**:307 (1982).
20. B. Shraiman, C. E. Wayne, and P. C. Martin, *Phys. Rev. Lett.* **46**:935 (1981).
21. M. J. Feigenbaum and B. Hasslacher, *Phys. Rev. Lett.* **49**:605 (1982).
22. A. B. Rechester and R. B. White, *Phys. Rev.* **A27**:1203 (1983).
23. H. D. J. Abarbanel and P. E. Latham, *Phys. Lett.* **89A**:55 (1982).
24. S. P. Hirshman and J. C. Whitson, *Phys. Fluids* **25**:967 (1982).
25. R. V. Jensen and C. R. Myers, *Phys. Rev.* (1985) (to appear).
26. R. Shaw, *Z. Naturforsh.* **36A**:80 (1981).
27. G. Bennetin, L. Galgani, and J. M. Strelcyn, *Phys. Rev.* **A14**:2338 (1979).
28. Ya. B. Pesin, *Russ. Math. Surveys* **32**:55 (1977).
29. A. J. Lichtenberg and M. A. Lieberman, *Regular and Stochastic Motion* (Springer, New York, 1983).
30. M. V. Jakobson, *Comm. Math. Phys.* **81**:39 (1981).
31. C. Grebogi, E. Ott, and J. Yorke, *Physica* **7D**:181 (1983).

32. T. Geisel and J. Nierwetberg, *Phys. Rev. Lett.* **48**:7 (1982).
33. M. Kac, *Ann. Math.* **47**:33 (1946).
34. J. Mathews and R. L. Walker, *Mathematical Methods of Physics* (W. A. Benjamin, Menlo Park, California, 1970), p. 186.
35. B. V. Chirikov, *Phys. Rep.* **52**:263 (1979).